



Contents lists available at ScienceDirect

# International Journal of Solids and Structures

journal homepage: [www.elsevier.com/locate/ijsolstr](http://www.elsevier.com/locate/ijsolstr)



## Discontinuous plastic flow in superconducting multifilament composites

J. Tabin <sup>a,b,\*</sup>, B. Skoczeń <sup>a</sup>, J. Bielski <sup>a</sup>



<sup>a</sup> Institute of Applied Mechanics, Faculty of Mechanical Engineering, Cracow University of Technology, 31-864 Cracow, Poland

<sup>b</sup> Institute of Fundamental Technological Research, Polish Academy of Sciences, 02-106 Warsaw, Poland

### ARTICLE INFO

#### Article history:

Received 13 February 2020

Received in revised form 20 May 2020

27 May 2020

Available online 4 June 2020

#### Keywords:

Superconductor

Plastic deformation

Cryogenic temperatures

Constitutive model

### ABSTRACT

Modern superconducting intermetallic materials (e.g. NbTi, Nb<sub>3</sub>Sn) are used to build conductors composed of a matrix and the superconductor strands. One of the most popular materials for matrix is copper, because of its excellent physical and mechanical properties at extremely low temperatures. Ductile OFE copper stabilizes, on one hand, the mechanical response of brittle superconductor strands and, on the other hand, takes over the electrical charge in case of quench (resistive transition). Thus, the composite structure of modern conductors used to build the coils of superconducting magnets is fully justified. Such a composite structure results in common deformation of the matrix and the strands when winding the coils and during the operation, when the coils are subjected to the prestress and to the Lorentz forces at extremely low temperatures (liquid or superfluid helium). When the loads are large enough, the copper-superconductor strands composite is subjected to inelastic deformation, including moderately large plastic strains. It is known, that copper and superconductor strands exhibit the so-called discontinuous plastic flow (DPF) at extremely low temperatures, that results in abrupt drops of stress against strain of different amplitude and frequency. In order to describe correctly the behaviour of composite superconductors at extremely low temperatures, a constitutive model of DPF has been developed and applied to both components: matrix and strands. The results of numerical analysis are compared with the experiments, carried out in dedicated cryostat containing liquid helium and the relevant instruments.

© 2020 The Authors. Published by Elsevier Ltd. This is an open access article under the CC BY license (<http://creativecommons.org/licenses/by/4.0/>).

## 1. Introduction

Superconducting wires are usually composed of brittle superconductor strands (e.g. NbTi, Nb<sub>3</sub>Sn), embedded in a ductile matrix (Devered, 2004; Zhang et al., 2019). One of the most popular materials used for matrix is copper, because of its excellent physical and mechanical properties at extremely low temperatures, including low electrical and thermal resistance and ductility. OFE copper stabilizes the mechanical response of brittle superconductor strands, allowing for larger deformations. Also, it takes over the electrical charge in case of quench, that means resistive transition in the superconductor strands. Moreover, reasonably good thermal conductivity at extremely low temperatures enables to cool down the superconductor strands back to their operational temperature in a fast way. The composite structure of modern conductors is therefore rational, and the ratio of superconductor to copper cross-section is close to an optimum. The composite superconducting wires are used to build the coils of the superconducting magnets. The composite structure leads to common deformation of

the matrix and the strands, both at warm when winding the coils, and during the operation at extremely low temperatures when the coils are subjected to the prestress and to the Lorentz forces. When the loads are large enough to induce stresses higher than the yield stress, the composite is subjected to moderately large plastic deformation, which induces the residual deformation. It is therefore crucial to study inelastic behaviour of the superconductor wires, in order to predict the extent of plastic deformation and the value of residual strain. It is quite known (Koch and Easton, 1977; Pustovalov, 2008; Skoczeń et al., 2014), that both copper and the superconductor strands exhibit the so-called discontinuous plastic flow (DPF, serrated yielding) when strained at extremely low temperatures. DPF manifests itself by the abrupt drops of stress against strain (or time), of the amplitude and the frequency depending on the material tested. In particular, the amplitude and the frequency of stress oscillations is different for copper and for the superconductor strands. Discontinuous plastic flow may have significant impact on the behaviour of the superconducting wires above the yield stress, including the occurrence of quench, therefore it needs to be studied from the point of view of materials science and mechanics. In order to describe the behaviour of composite superconductor wires at extremely low temperatures, a complex

\* Corresponding author.

E-mail address: [jtabin@ippt.pan.pl](mailto:jtabin@ippt.pan.pl) (J. Tabin).

constitutive model has to be developed, including the plastic flow discontinuities. It has to take into account the behaviour of both components: the matrix and the strands. The homogenization scheme has to be adopted in order to compute the overall tangent stiffness of the composite containing the superconducting fibres. Some initial work on this was carried out by Koch and Easton (1977), they have used simple mixing law. The same approach was used by Thilly et al. (2009) to identify the mechanical properties of a nanocomposite wires composed of Cu matrix embedding Nb nanotubes. Such a composite represents high strength-high conductivity materials for non-destructive high field magnets. The authors carried out cyclic loading - unloading tests during which the microstructural evolution was investigated by means of the X-ray diffraction method. Based on the results, the elasto-plastic regimes were identified and the "tangent moduli" were obtained for each of them. The Authors considered only elastic response of the Nb nanotubes. Moreover new criterion for determining the macro-yield stress was presented.

In order to identify a strengthening mechanism of nanostructured Cu-Nb-based wires and Cu/Nb/Cu nano-filamentary wires, Vidal et al. (2009) carried out in-situ tensile tests during neutron diffraction. Presented results revealed the load transfer from the Cu matrix to the Nb nanotubes.

More sophisticated approach to characterize a elasto-plastic behaviour of architectured and nanostructured Cu-Nb composite wires was proposed by Gu et al. (2017, 2019). The Authors presented a comprehensive study of the effective elasto-plastic behaviour of nanostructured Cu-Nb composite wires by using two different approaches to model the microstructural features: full-field finite elements method with periodic boundary conditions and mean-field  $\beta$ -model. Nevertheless, presented models do not take into account the plastic flow instability behaviour of polycrystalline materials at cryogenic temperatures, near to absolute zero.

In this paper a new multiscale model of DPF in superconducting multifilament composites is presented. In order to obtain the overall tangent stiffness of the composite two approaches have been used: the mixing law and the mean field methods. Moreover, it has to be based on a number of assumptions related to the coexistence of both components in the same unidirectional composite, like the coherence of the copper-superconductor interface, and the same strain. The assumptions will be listed and justified in the section dedicated to the model of the composite.

## 2. Discontinuous plastic flow (DPF) at extremely low temperatures

The discontinuous plastic flow has been studied, mainly experimentally, by many authors, among them Basinski, 1957, Schwarz and Mitchell, 1974, Reed et al., 1988, Reed and Walsh, 1988, or Zaiser and Hahner, 1997. It was first Basinski, who developed a consistent approach to the serrated yielding based on a thermodynamic approach. He observed that the specific heat and the thermal conductivity tend to zero with temperature, which is consistent with the 3rd principle of thermodynamics. Moreover, by assuming the adiabatic heating hypothesis, he noted that "any fast dissipative process that occurs at extremely low temperature leads to increase of local temperature, which results in a drastic decrease of the flow stress". Thus, the drops of stress were attributed to the variations of the flow stress, resulting from the oscillations of temperature, under quasi adiabatic conditions. This approach was followed by a number of authors, however, the real breakthrough came with the experiments where the load was measured directly on the sample.

The question of other possible explanations was raised by Wessel (1957), and Tabachnikova et al. (1984), who postulated

that if the flow stress at extremely low temperatures is sufficiently high, it can induce some sort of avalanche-like process of multiplication of mobile dislocations. Such a process can potentially lead to the plastic flow instabilities.

A significant step forward has been made by Obst and Nyilas (1991, 1998), who performed a series of experiments with the load measured directly on the sample (Fig. 1). Following the way of thinking of Seeger (1957), the Authors postulated that the cause of discontinuous plastic flow is related to the pile-ups of dislocations on the internal lattice barriers (e.g. the Lomer-Cottrell locks, the Cottrell atmospheres, the Suzuki locks, etc.) The presence of the dislocation pile-ups on the barriers leads to the stress concentrations of the order of theoretical shear strength. As soon as the local resolved shear stress at the head of dislocation pile-up reaches a critical value, a catastrophic process of breaking the barrier takes place, and the released dislocations can freely glide away. If such a process takes simultaneously place in many locations in the lattice, the effect is collective and massive, and results in macroscopic slip equivalent to sudden jump of strain and drop of stress. Thus, according to Obst and Nyilas, the DPF is of mechanical origin. Similar experiments were performed by Tabin, Skoczen and Bielski (2016, 2017, 2019) with even higher precision and better instrumentation, leading to confirmation of the hypothesis expressed by Obst and Nyilas. Clearly, the thermal response is crucial, and has to be taken into account by analysing the thermodynamic background, characteristic of extremely low temperatures (Fig. 2).

The thermodynamic background is strictly related to the 3rd principle of thermodynamics which postulates that the entropy tends to zero with temperature. Similar behaviour is attributed to the specific heat and the thermal conductivity that both tend to zero with temperature. Based on the literature data (Bauer et al., 2007; Marquardt et al., 2000; Rossi and Sorbi, 2006), the estimates of the specific heat and of the thermal conductivity for OFE Cu and for superconducting wires (NbTi, Nb<sub>3</sub>Sn) were obtained in a wide range of temperatures. Both thermodynamic functions are non-linear with temperature, and tend to 0 when the temperature approaches absolute zero, as shown in Figs. 3 and 4. It is worth pointing out, that the thermal conductivity of OFE Cu is still quite high in the range above 1 K.

As the thermodynamic functions tend to 0 with temperature, the so called thermodynamic instability takes place. The derivative of heat with respect to temperature is equal to the product of mass and specific heat of the sample:

$$\frac{dQ}{dT} = mC_V \quad (1)$$

Computing the inverse derivative, one obtains:

$$\frac{dT}{dQ} = \frac{1}{mC_V} \quad (2)$$

Knowing that:

$$C_V \xrightarrow{T \rightarrow 0} 0 \quad (3)$$

one obtains:

$$\frac{dT}{dQ} \xrightarrow{T \rightarrow 0} \infty \quad (4)$$

This means that in the proximity of absolute zero an arbitrary small dissipation of energy in the lattice will produce significant increase of temperature. Among possible sources of energy dissipation, such processes like inelastic deformation or micro-damage evolution have to be accounted for. In particular, plastic deformation represented by massive motion of dislocations in the lattice or by a localized effect in the form of macroscopic slip, will produce enough energy to raise the temperature by several Kelvins.

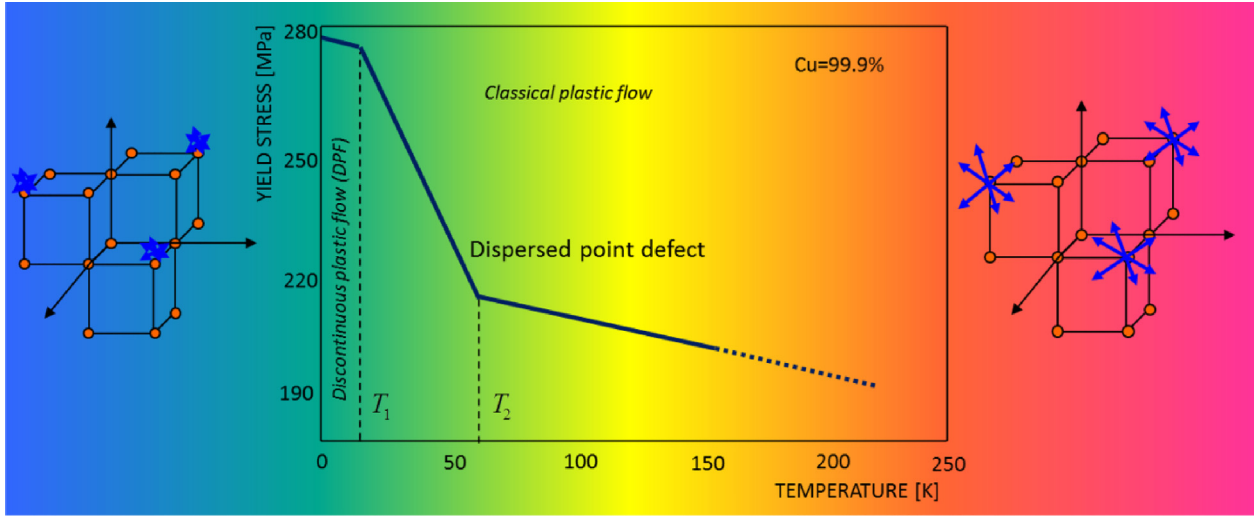


**Fig. 1.** DPF at extremely low temperatures (below  $T_1$ ), illustrated by means of the plot of yield stress against temperature for Cu 99.9% (Obst and Nyilas, 1991).

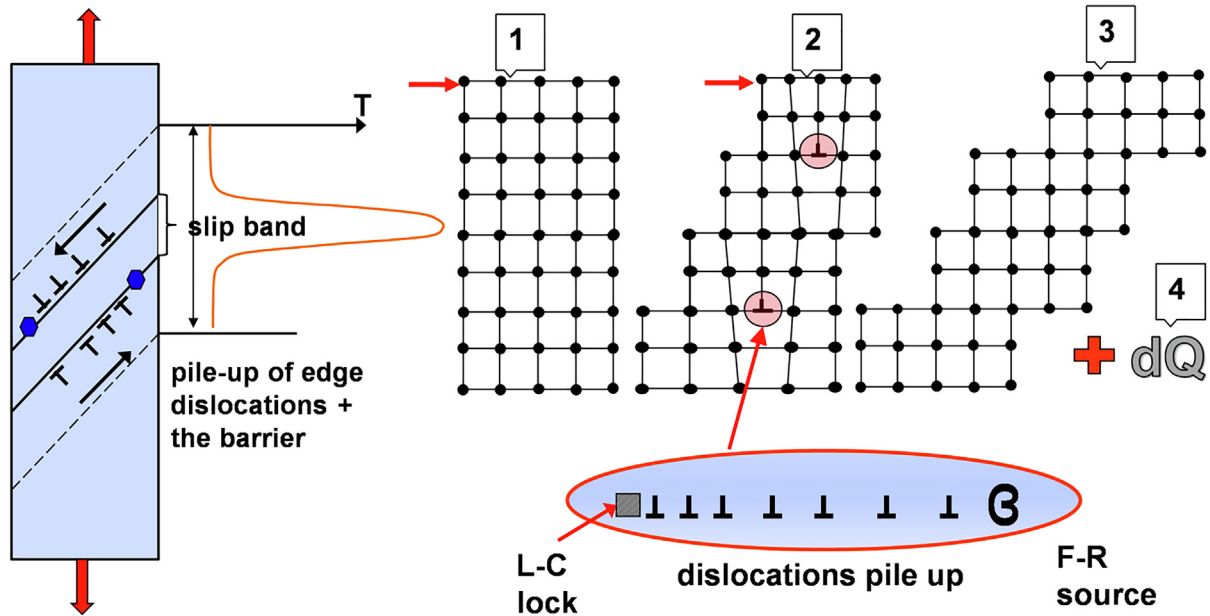


**Fig. 2.** The mechanism of DPF in the context of shear band propagation.

Thermodynamic instability plays an important role in the discontinuous plastic flow, since it affects the excitation of lattice in the proximity of the macroscopic slip resulting from the collapse of local lattice barriers under the stresses caused by the pile-ups of dislocations.

### 3. The constitutive model of DPF

The constitutive model of discontinuous plastic flow is physically based, which means that the main mechanisms of plastic flow related to the motion of dislocations have been taken into account. Two mechanisms are considered: redistributed motion of dislocations in the whole volume of the RVE, and localized macroscopic slip due to the motion of released dislocations after a collective collapse of the lattice barriers under the shear stresses developed in the pile-ups of dislocations. Such a model of DPF has been developed by Skoczen et al., since 2008 for single materials, such as the stainless steel (304, 316LN, etc), the OFC copper and C15100. In this

paper a constitutive model of DPF for composites has been proposed. It is assumed that the plastic flow can take place both in the matrix, and in the superconducting fibres. Local behaviour of the matrix and the superconducting fibres is defined by the relevant tangent stiffness operators, computed at each stage of the deformation process. The behaviour of the composite results from the behaviour of the matrix and the fibres. In particular, the model of unidimensional composite is based on the definition of the tangent stiffness operator resulting from the operators computed for the matrix and for the fibres. The model is developed at the mesoscopic level, and the results are imported to the macroscopic framework of classical plasticity, including the associated flow rule.

#### 3.1. The kinetics of single serration and the criterion of drop of stress

The kinetics of DPF is based on the rate of production of lattice barriers as a function of plastic flow intensity. It is assumed that the probability of lattice barrier formation is strictly related to

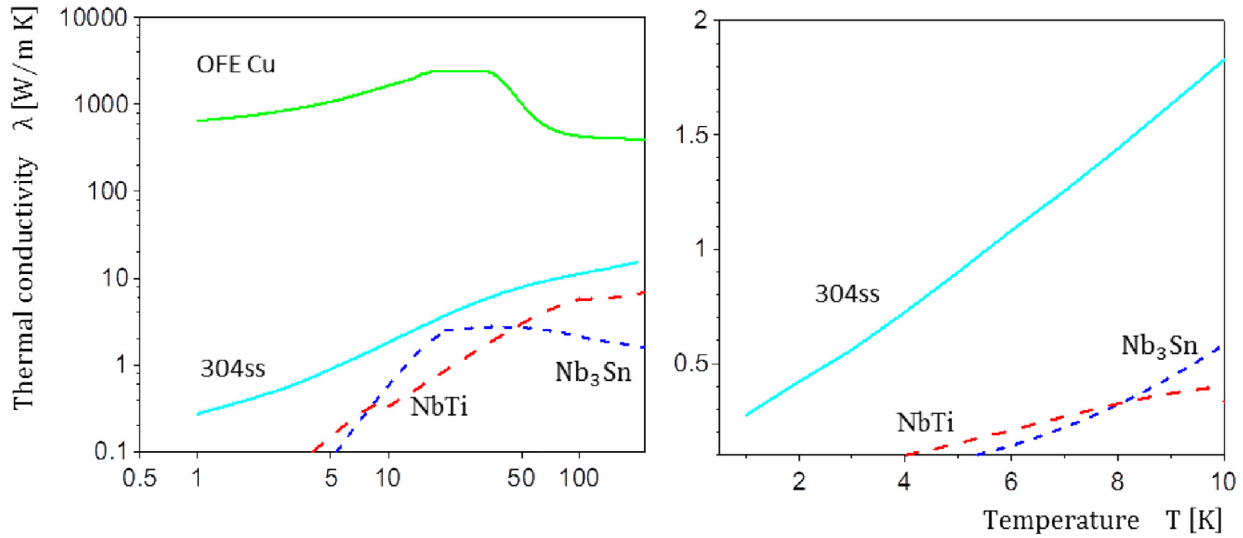


**Fig. 3.** Thermal conductivity of OFE Cu, low-temperatures superconductors (NbTi, Nb<sub>3</sub>Sn), and 304 stainless steel as a function of temperature (Bauer et al., 2007; Marquardt et al., 2000; Rossi and Sorbi, 2006).

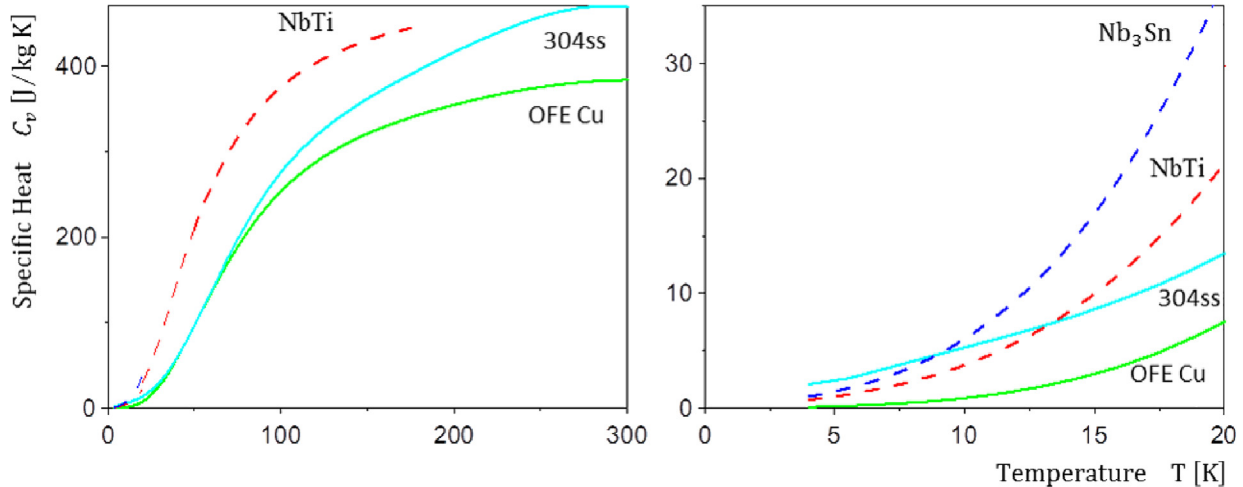


**Fig. 4.** Specific heat of OFE Cu, low-temperatures superconductors (NbTi, Nb<sub>3</sub>Sn), and 304 stainless steel as a function of temperature (Bauer et al., 2007; Marquardt et al., 2000; Rossi and Sorbi, 2006).

the intensity of plastic strains, reflected by the accumulated plastic strain (Skoczeń, 2008):

$$\frac{dB}{dt} = F_B^+(\rho, \sigma, T) \frac{dp}{dt} H(p - p_B) \quad (5)$$

where  $B$  denotes the number of lattice barriers per unit surface,  $F_B^+$  is a function reflecting the influence of dislocations density, stress and temperature, and  $p$  is the accumulated plastic strain.  $H(..)$  stands for the Heaviside function and  $p_B$  represents the threshold above which the lattice barriers evolve. Assuming, that the threshold has been reached, one obtains:

$$dB = F_B^+ dp \quad (6)$$

here, the accumulated plastic strain is expressed by:

$$(dp)^2 = \frac{2}{3} d e_{ij}^p d e_{ij}^p \quad (7)$$

In order to compute the shear stress at the head of dislocation pile-up, firstly the density of dislocations has to be determined. Local dislocations density obeys the following law (Kocks and Mecking, 2003; Mecking and Kocks, 1981):

$$d\rho_{\gamma\gamma} = d\rho_{\gamma\gamma}^+ + d\rho_{\gamma\gamma}^- \quad (8)$$

where (+) denotes production of dislocations, whereas, (-) denotes annihilation of dislocations. Given the fact, that the production part is inversely proportional to the mean free path of dislocation in the lattice:

$$d\rho_{\gamma\gamma}^+ = (\lambda b)^{-1} \quad (9)$$

and the mean free path is expressed by:

$$\lambda^{-1} = \sum_i \lambda_i^{-1} \quad (10)$$

one obtains:

$$\lambda^{-1} = d^{-1} + k_{c1} \rho^{0.5} \quad (11)$$

where  $k_{c1}$  is a constant, and  $d$  denotes the grain size. The annihilation term is expressed by the following equation:

$$d\rho_{\gamma\gamma}^- = -k_a \rho \quad (12)$$

with  $k_a$  being the dislocations annihilation constant. Finally, the dislocations density is expressed by the following equation:

$$d\rho_{,\gamma} = (db)^{-1} + k_{c1}b^{-1}\rho^{0.5} - k_a\rho \quad (13)$$

It is now assumed that the elastic strains are negligible when compared to plastic strains, and the local shear stress and the local resolved shear strain can be converted to the macroscopic stress and strain, respectively, by means of the Taylor factor  $M$ :

$$\sigma = M\tau; \gamma = M\varepsilon$$

In the light of the above micro/macro relationship one obtains:

$$d\rho_{,\nu p} = M \left[ (db)^{-1} + k_{c1}b^{-1}\rho^{0.5} - k_a\rho \right] \quad (15)$$

Now, the average shear stress in the lattice can be computed:

$$\tau = \tau_0 + \mu\alpha b\rho^{0.5} \quad (16)$$

which reflects the frictional term, and the term related to interaction of dislocations, determined by the shear modulus  $\mu$  and the coefficient  $\alpha$ . Finally, the shear stress at the head of dislocations pile-up is expressed by:

$$\tau_e = \pi(1-\nu)(b\mu)^{-1}\bar{\lambda}\tau^2 \quad (17)$$

where the mean free path of dislocation represents the distance between source and a lattice barrier:

$$(\bar{\lambda})^{-1} = \lambda^{-1} + k_{c2}B^{0.5} \quad (18)$$

Here,  $B$  is computed from the Eq. (5) evolution equation. The pair of variables  $(B, \tau_e)$  is sufficient to determine the conditions of drop of stress due to the catastrophic failure of internal lattice barriers, when the number of barriers and the level of shear stresses at the heads of dislocation pile-ups are large enough (Skoczeń, 2008):

$$\frac{B - B_{min}}{B_{cr} - B_{min}} = \frac{\tau_e - \tau_{cr}}{\tau_{min} - \tau_{cr}}; \quad \tau \geq \tau_{min} \wedge B \geq B_{min} \quad (19)$$

On the other hand, the following conditions hold:

$$\tau < \tau_{min} \Rightarrow B = B_{cr}$$

$$B < B_{min} \Rightarrow \tau_e = \tau_{cr} \quad (20)$$

The above criterion is piecewise linear, and determines the conditions of single serration for a process that starts with the variables  $(B, \tau_e)$  obtained from the previous serration. The values:

$$B_{min} = \alpha_B B_{cr}; \quad \tau_{min} = \alpha_\tau \tau_{cr} \quad (21)$$

were obtained as a function of the critical values. As soon as the criterion is fulfilled, the drop of stress takes place. The magnitude of drop of stress is determined by means of the following equation (Skoczeń et al., 2010):

$$\Delta\sigma = M\mu\alpha b(\sqrt{\rho} - \sqrt{\rho_0}) \quad (22)$$

and depends on the density of dislocations before and after the serration. It is worth pointing out, that the drop of stress results from a macroscopic slip between two portions of lattice, each of them being unloaded. The elastic unloading of both lattice portions involved in the macroscopic slip is equivalent to the amount of slip in the following way:

$$\Delta\varepsilon^{ps} = \frac{\Delta\sigma}{E} \quad (23)$$

where  $E$  denotes the Young modulus.

Thus, the plastic deformation contains essentially two components: the redistributed deformation based on the motion of dislocations ( $\Delta\varepsilon^{pd}$ ), and highly localized plastic slip ( $\Delta\varepsilon^{ps}$ ). In the present model these two effects are superposed, so that:

$$\Delta\varepsilon^p = \Delta\varepsilon^{pd} + \Delta\varepsilon^{ps} \quad (24)$$

### 3.2. Multiaxial constitutive model

In the case of multiaxial constitutive model, the general constitutive equation reads:

$$\sigma_{ij} = E_{ijkl} \left( \varepsilon_{kl} - \varepsilon_{kl}^{pd} - \varepsilon_{kl}^{ps} \right) \quad (25)$$

where  $E_{ijkl}$  is the 4th order elasticity tensor. The plastic flow is represented by the yield surface in the following form:

$$f_y = J_2(s_{ij} - X_{ij}) - R - \sigma_0; \quad J_2(s_{ij} - X_{ij}) = \left( \frac{3}{2}(s_{ij} - X_{ij})(s_{ij} - X_{ij}) \right)^{0.5} \quad (26)$$

where  $J_2$  is the second invariant of the stress tensor,  $s_{ij}$  denotes the deviatoric stress,  $X$  denotes the back stress,  $R$  denotes the isotropic hardening variable, and  $\sigma_0$  is the yield stress. In order to derive the plastic strain increment, the associated flow rule is assumed:

$$d\varepsilon_{ij}^{pd} = d\lambda n_{ij} = d\lambda \frac{\partial f_y}{\partial \sigma_{ij}} \quad (27)$$

where  $n_{ij}$  denotes vector normal to the yield surface. The evolution laws for the back stress, and for the isotropic hardening variable, read:

$$dX_{ij} = \frac{2}{3}C_X d\varepsilon_{ij}^{pd}; \quad dR = C_R dp \quad (28)$$

where  $C_X$  and  $C_R$  denote the kinematic and the isotropic hardening moduli, respectively. As soon as the plastic strain increment is obtained, the parameter  $B$  is computed, and the serration criterion is checked.

In order to establish a proportion between the kinematic and the isotropic hardening, the Baushinger parameter  $\beta$  can be introduced:

$$\beta = \frac{\sigma^+ - \sigma^-}{2(\sigma^+ - \sigma_0)}, \quad 0 \leq \beta \leq 1 \quad (29)$$

where  $\sigma^+$  denotes the stress level at which the unloading process starts,  $\sigma^-$  is the yield stress at the reverse active process and  $\sigma_0$  is the yield point. The Baushinger parameter varies between 0 (isotropic hardening, no Baushinger effect) and 1 (kinematic hardening, pure Baushinger effect). In view of foregoing, the evolution of isotropic hardening and kinematic hardening depend on Baushinger parameter in the following way:

$$dR = \beta(1-\beta)C_R dp = C_R dp, \quad dX_{ij} = \frac{2}{3}\beta C_{X0} d\varepsilon_{ij}^{pd} = \frac{2}{3}C_X d\varepsilon_{ij}^{pd} \quad (30)$$

In order to define the kinematic and isotropic hardening variables the integration with respect to the accumulated plastic strain and plastic strain are required.

### 3.3. DPF in the composite containing long fibres

A composite consisting of the superconducting wires embedded in the Cu matrix is considered. Both materials exhibit the discontinuous plastic flow so that the composite is subjected to two types of serrations: in the strands and in the matrix. Each material is considered elastic-plastic with linear hardening. In order to determine the equivalent tangent stiffness operator, a homogenization algorithm is applied. Four possible cases in terms of the behaviour of matrix and strands are studied: elastic-elastic (I), plastic-elastic (II), elastic-plastic (III) and plastic-plastic (IV). In each case, the tangent stiffness operator in the isotropic or quasi-isotropic form will be used. In what follows, the matrix will be denoted (1) and the strands will be denoted (2).

### 3.3.1. The elastic-elastic case

The elastic behaviour of the matrix is represented by the 4th order stiffness tensor:

$$E_{ijkl}^1 = 3k_1 J_{ijkl} + 2\mu_1 K_{ijkl} \quad (31)$$

where

$$\mu_1 = \frac{E_1}{2(1+v_1)}; \quad k_1 = \frac{E_1}{3(1-2v_1)} \quad (32)$$

whereas, the elastic behaviour of the strands is represented by the following tensor:

$$E_{ijkl}^2 = 3k_2 J_{ijkl} + 2\mu_2 K_{ijkl} \quad (33)$$

where

$$\mu_2 = \frac{E_2}{2(1+v_2)}; \quad k_2 = \frac{E_2}{3(1-2v_2)} \quad (34)$$

The resultant stiffness tensor reads:

$$E_{ijkl}^{ee} = 3k_H J_{ijkl} + 2\mu_H K_{ijkl} \quad (35)$$

and the stress increment can be computed in the following way:

$$d\sigma_{ij} = E_{ijkl}^{ee} d\varepsilon_{kl} \quad (36)$$

In order to obtain the resultant stiffness tensor, the Mori-Tanaka homogenization scheme will be used:

$$\begin{aligned} 3k_H + 3k^* &= \left\{ \frac{1-\xi}{3(k_1+k^*)} + \frac{\xi}{3(k_2+k^*)} \right\}^{-1} \\ 2\mu_H + 2\mu^* &= \left\{ \frac{1-\xi}{2(\mu_1+\mu^*)} + \frac{\xi}{2(\mu_2+\mu^*)} \right\}^{-1} \\ k^* &= \frac{4}{3}\mu_1; 2\mu^* = \mu_1 \frac{9k_1+8\mu_1}{3(k_1+2\mu_1)} \end{aligned} \quad (37)$$

where  $\xi$  denotes the volume fraction of strands in the composite.

### 3.3.2. The plastic-elastic case

In this case the matrix is subjected to plastic flow, whereas, the strands remain elastic. The tangent stiffness operator for the matrix reads:

$$E_{ijkl}^{t1} = 3k_1 J_{ijkl} + 2\mu_1 \left( K_{ijkl} - \frac{n_{ij} \otimes n_{kl}}{1 + \frac{C}{3\mu_1}} \right) \quad (38)$$

where the second term in the bracket contains dyadic product of the tensors representing normal to the yield surface. In order to use the homogenization algorithm, the tangent stiffness operator has to be projected into the space of isotropic operators, and takes the form:

$$E_{ijkl}^{t1} = 3k_{t1} J_{ijkl} + 2\mu_{t1} K_{ijkl} \quad (39)$$

where

$$\mu_{t1} = \frac{E_{t1}}{2(1+v_1)}; \quad k_{t1} = \frac{E_{t1}}{3(1-2v_1)}; \quad E_{t1} = \frac{E_1 C_1}{E_1 + C_1} \quad (40)$$

Here,  $E_1$  denotes the elasticity modulus, and  $C_1$  denotes the hardening modulus for copper. The tangent stiffness operator can be reduced to the following form:

$$E_{ijkl}^{t1} = \eta_1 E_{ijkl}^1 \eta_1 = \frac{C_1}{E_1 + C_1} \quad (41)$$

The elastic behaviour of strands is represented by the same stiffness tensor like in the previous case:

$$E_{ijkl}^2 = 3k_2 J_{ijkl} + 2\mu_2 K_{ijkl} \quad (42)$$

By performing the homogenization according to the following scheme:

$$\begin{aligned} 3k_H + 3k^* &= \left\{ \frac{1-\xi}{3(\eta_1 k_1+k^*)} + \frac{\xi}{3(\eta_2 k_2+k^*)} \right\}^{-1} \\ 2\mu_H + 2\mu^* &= \left\{ \frac{1-\xi}{2(\eta_1 \mu_1+\mu^*)} + \frac{\xi}{2(\eta_2 \mu_2+\mu^*)} \right\}^{-1} \\ k^* &= \frac{4}{3}\eta_1 \mu_1; 2\mu^* = \eta_1 \mu_1 \frac{9k_1+8\mu_1}{3(k_1+2\mu_1)} \end{aligned} \quad (43)$$

one obtains the resultant tangent stiffness operator in the following form:

$$E_{ijkl}^{pe} = 3k_H J_{ijkl} + 2\mu_H K_{ijkl} \quad (44)$$

and the stress increment reads:

$$d\sigma_{ij} = E_{ijkl}^{pe} d\varepsilon_{kl} \quad (45)$$

### 3.3.3. The elastic-plastic case

The elastic-plastic case is similar to the previous one, however, the roles are inverted. The behaviour of the matrix is elastic:

$$E_{ijkl}^1 = 3k_1 J_{ijkl} + 2\mu_1 K_{ijkl} \quad (46)$$

and the response of the strands is plastic:

$$E_{ijkl}^{t2} = \eta_2 E_{ijkl}^2; \quad \eta_2 = \frac{C_2}{E_2 + C_2} \quad (47)$$

The relevant set of equations for the Mori-Tanaka algorithm reads:

$$\begin{aligned} 3k_H + 3k^* &= \left\{ \frac{1-\xi}{3(k_1+k^*)} + \frac{\xi}{3(\eta_2 k_2+k^*)} \right\}^{-1} \\ 2\mu_H + 2\mu^* &= \left\{ \frac{1-\xi}{2(\mu_1+\mu^*)} + \frac{\xi}{2(\eta_2 \mu_2+\mu^*)} \right\}^{-1} \\ k^* &= \frac{4}{3}\mu_1; 2\mu^* = \mu_1 \frac{9k_1+8\mu_1}{3(k_1+2\mu_1)} \end{aligned} \quad (48)$$

and the resultant tangent stiffness operator reads:

$$E_{ijkl}^{ep} = 3k_H J_{ijkl} + 2\mu_H K_{ijkl} \quad (49)$$

with the stress increment equal to:

$$d\sigma_{ij} = E_{ijkl}^{ep} d\varepsilon_{kl} \quad (50)$$

It is worth pointing out that in Cu-NbTi composite elastic-plastic case does not appear. Nevertheless, presented consideration can be used for wide range of composite.

### 3.3.4. The plastic-plastic case

Finally, the plastic-plastic case represents the simultaneous plastic behaviour in both components of the composite. Thus, one obtains for the matrix:

$$E_{ijkl}^{t1} = \eta_1 E_{ijkl}^1; \quad \eta_1 = \frac{C_1}{E_1 + C_1} \quad (51)$$

and for the strands:

$$E_{ijkl}^{t2} = \eta_2 E_{ijkl}^2; \quad \eta_2 = \frac{C_2}{E_2 + C_2} \quad (52)$$

The homogenization algorithm is reflected by:

$$\begin{aligned} 3k_H + 3k^* &= \left\{ \frac{1-\xi}{3(\eta_1 k_1+k^*)} + \frac{\xi}{3(\eta_2 k_2+k^*)} \right\}^{-1} \\ 2\mu_H + 2\mu^* &= \left\{ \frac{1-\xi}{2(\eta_1 \mu_1+\mu^*)} + \frac{\xi}{2(\eta_2 \mu_2+\mu^*)} \right\}^{-1} \\ k^* &= \frac{4}{3}\eta_1 \mu_1; 2\mu^* = \eta_1 \mu_1 \frac{9k_1+8\mu_1}{3(k_1+2\mu_1)} \end{aligned} \quad (53)$$

and the stress increment reads:

$$d\sigma_{ij} = E_{ijkl}^{pp} d\varepsilon_{kl} \quad (54)$$

All the above cases may occur as a function of the mutual properties of the matrix and the strands.

#### 4. Experimental validation of DPF in superconducting multifilament composites

##### 4.1. Experimental set-up for tensile test at cryogenic temperatures

Kinematically controlled uniaxial tensile tests at the liquid helium temperature (4.2 K) were performed for OFE Cu wires, OFE Cu flat specimen and for a superconducting multifilament composite Cu-NbTi. The stress-strain curve for NbTi specimen was adopted from Koch and Easton (1977).

Tensile tests were carried out on the unique experimental set-up. The general schemes of the experimental set-up, as well as the cryostat interior, are presented in Fig. 5. The cryostat with the specimen and the transducers were mounted between the grips of the tensile test machine. The cryogen (liquid helium) was transferred to the cryostat by means of the transfer line, until the specimen with the transducers was immersed in the medium. The level of the cryogen was indicated by a thermistor mounted inside the cryostat. The kinematically controlled uniaxial tensile tests were carried out with the cross-head speed of 0.1 cm/min. During the tests, the elongation of the specimen was measured by means of the clip-on extensometers, the applied force by means of the piezoelectric transducer mounted just behind the specimen. The temperature of the specimen during plastic deformation was measured by means of the thermistor mounted on it.

It is worth pointing out, that the clip-on extensometers are recommended by the international standards (ISO 19819, Metallic materials, Tensile Testing in Liquid Helium). For the present work very light Nyilas-type extensometers were used, which were specifically designed for the superconducting wires and filaments (Shin et al., 2008). Nevertheless, during the tensile test in the liquid helium, such dynamic effect in material like the DPF can generate vibrations of the extensometers-specimen structure. It leads to erroneous interpretation of tensile test results. Simple approach to determine the dynamic properties of the extensometers-specimen structure was discussed by Tabin and Pracik (2015). Based on this approach, suitable clip-on extensometers were selected to perform the cryogenic tensile tests at extremely low temperatures (see Fig. 5).

The composite specimen for tensile test at cryogenic temperatures was severed from superconducting auxiliary busbars which are used to feed the “spoolpieces” – superconducting corrector magnets located in the main dipole in the Large Hadron Collider at CERN (Tock et al., 2004). These busbars consist of a rectangular shape copper conductor with NbTi filaments. The cross-section of tested specimen and the specimen grip system are presented in Fig. 6. The OFE Cu wire specimens were severed from cable tested in SMC (Short Model Coil).

The parameters of the superconducting multifilament composite, the NbTi wire, the OFE Cu wire and the OFE Cu flat specimen are presented in Table 1.

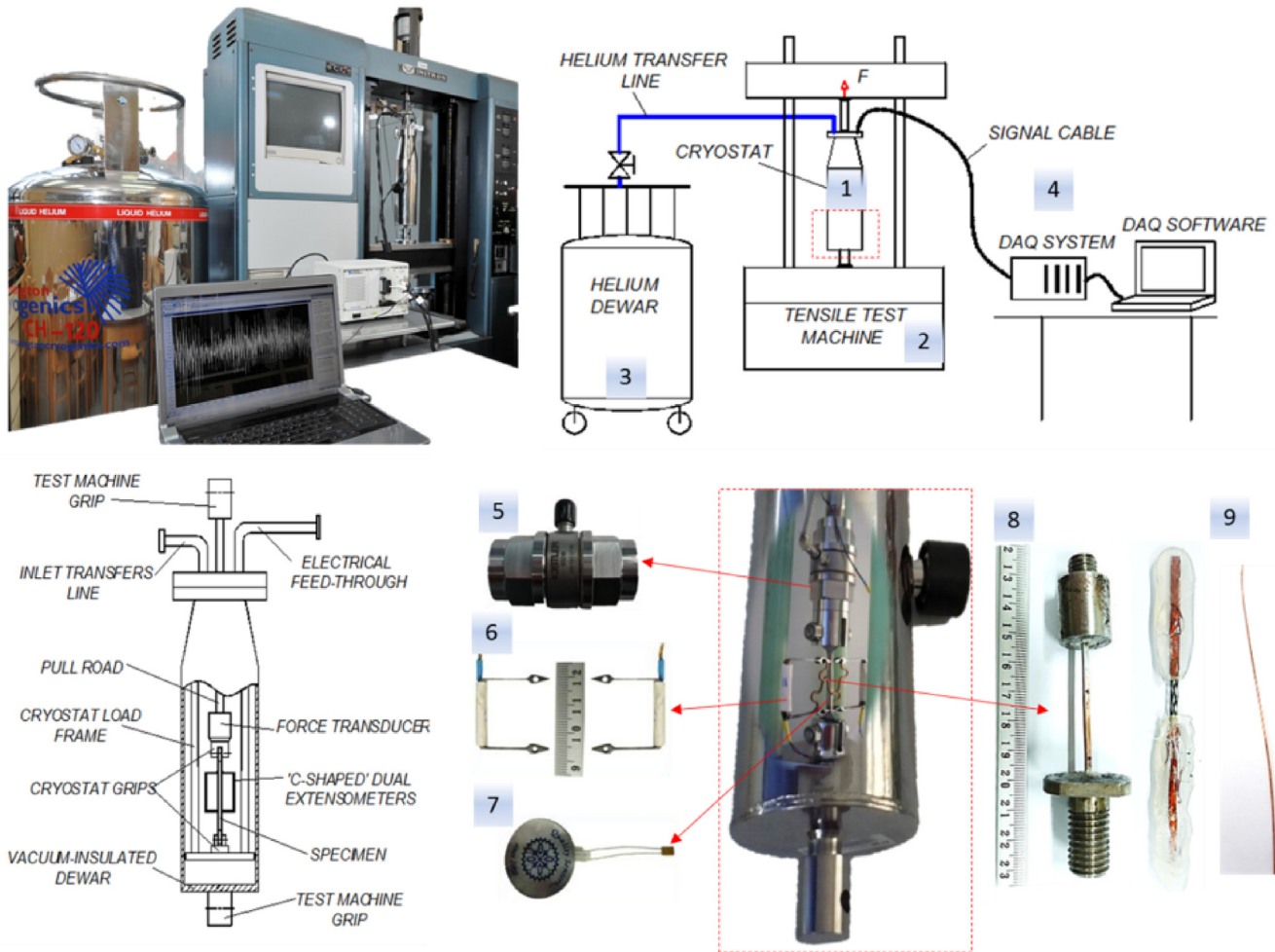


**Fig. 5.** Experimental set-up for tensile testing at extremely low temperatures; cryostat (1) equipped with the suitable instrumentation: quartz link (5), clip-on extensometers (6), thermometer (7), specimens: superconducting multifilament composite (8) and NbTi wire (9), DAQ system (4).

In our case the volume fraction of NbTi wires in composite is less than 15%, what has significant influence on composite behaviour, obviously. Such a ratio results from the fact that during resistive transition (quench) the heat transfer is mainly realised by copper matrix.

#### 4.2. Test results

Discontinuous plastic flow (DPF) was observed in the OFE Cu flat specimen during the kinematically controlled uniaxial tensile tests at 4.2 K. The uniform gauge section had the length of 25.4 mm, and the cross section of the gauge section was of 9.06 mm<sup>2</sup>. Based on the time responses of the extensometers and the force transducer the stress-strain curve for OFE Cu was obtained (Fig. 7).

During the monotonic tensile test, the recorded saw-tooth function of force is correlated in time with the step function of elongation, and the  $\delta$ -Dirac temperature distribution (Fig. 8b,c).

The time responses of transducers reflect the microstructural processes that occur inside the specimen. For instance, the massive failure of lattice barriers during DPF is followed by the fast motion of glissile dislocations in the lattice, thus the macroscopically abrupt drop of stress is observed. The heat released in the course of this process depends on the plastic work and the internal friction in the lattice, and it is reflected by the temperature distribution (Fig. 8). It is worth pointing out, that specific heat vanishes when the temperature approaches absolute zero (Fig. 4), thus small amount of heat generates drastic increase of temperature. It is the so-called thermodynamic instability, which is reflected during the test by the  $\delta$ -Dirac temperature peaks (see Chapter 3).

The maximum recorded temperature jump during DPF in OFE Cu specimen was about 6 K. It is much lower, compared to the austenitic stainless steel (304), where it is about 35 K (Tabin et al., 2016). The reason is that the thermal conductivity of copper specimen in liquid helium is significantly higher than the austenitic stainless steel (Fig. 3). Therefore, the relaxation stage is not observed in OFE Cu.

Each serration in the OFE Cu stress-strain curve (red curve in Fig. 9) has similar pattern: after initial elastic process (1) smooth plastic flow occurs (2), until the abrupt drop of stress (3) takes

**Table 1**

Geometrical parameters of Cu-NbTi composite, NbTi wire (Koch and Easton, 1977) and OFE Cu specimens.

Cu-NbTi (composite)	
Diameter of NbTi filament	43.1 $\mu$ m
Number of NbTi bundles	6
NbTi filaments in bundle	44
Area of NbTi filaments	0.39 mm <sup>2</sup>
Area of Cu matrix	2.63 mm <sup>2</sup>
Volume fraction of filaments in composite	0.148
<i>NbTi (wire)</i>	
Diameter of wire	0.45 mm
Area of wire	0.16 mm <sup>2</sup>
<i>OFE Cu (wire)</i>	
Diameter of wire	0.65 mm
Area of wire	0.33 mm <sup>2</sup>
<i>OFE Cu (flat specimen)</i>	
Type of cross section	rectangular
Area o cross section	9.06 mm <sup>2</sup>

place. Heat generated during DPF is reflected by the temperature distribution (blue curve). The experimental result indicates, that during third stage of DPF, the increment of plastic strain is related to sudden and collective motion of dislocations after the collapse of the lattice barriers (the steps on elongation curve, Fig. 8b). Hence, the mechanism of plastic deformation is different than in the classical continuous plastic flow (stage 2). Since the total value of strain in stage 3 remains constant, the increment of plastic part is equivalent to decrement of the elastic one and results in a drop of the stress value (Fig. 9).

The DPF effect was also observed in the OFE Cu wire specimen. The results of test at 4.2 K are presented in Fig. 10 (blue curve).

It is worth pointing out that the plastic flow instability reflected by the oscillations occurred relatively late in OFE Cu wire specimen (Fig. 10a). Moreover, the stress amplitude of serration in OFE Cu wire is much smaller than in the NbTi wire (Fig. 11). This fact is crucial for identification of DPF in the Cu-NbTi composite specimen. It is worth pointing out that there are metallographic evidence indicates that in annealed Nb-55-wt%Ti a systematic

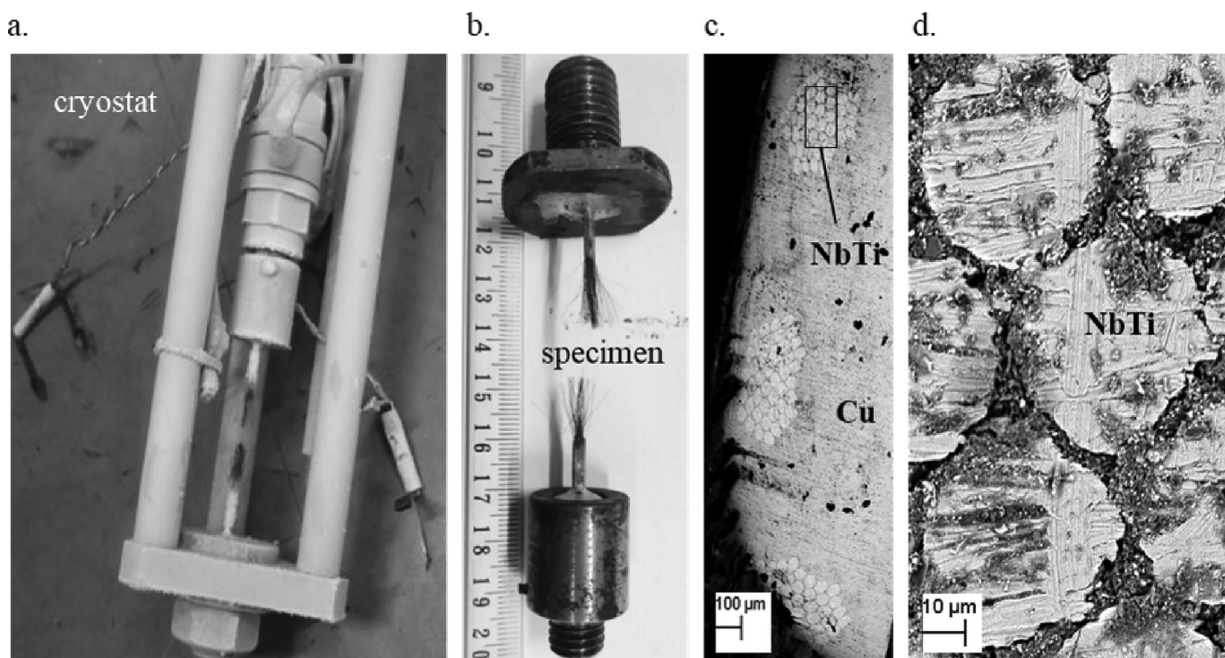


**Fig. 6.** a), b) Superconducting multifilament composite Cu-NbTi after the uniaxial tensile test at 4.2 K, c), d) cross-section of composite.

lattice transformation (twinning or martensitic) is induced at 76 K and 4 K (Read, 1978).

The results of uniaxial tensile test of composite specimen are presented in Fig. 12. The specimen consists of NbTi filaments, which are twisted together and embedded in an OFE Cu matrix (Fig. 6d).

The following mechanical parameters (Table 2) were identified during kinematically controlled uniaxial tensile test of Cu-NbTi specimen (stress-strain curve in Fig. 10):

where  $E_0$  is the initial elastic stiffness of composite,  $\sigma_0$  and  $E_h$  represent the stress and hardening modulus when plastic deformation occurs in the matrix (index 1) and then in the filaments (2).

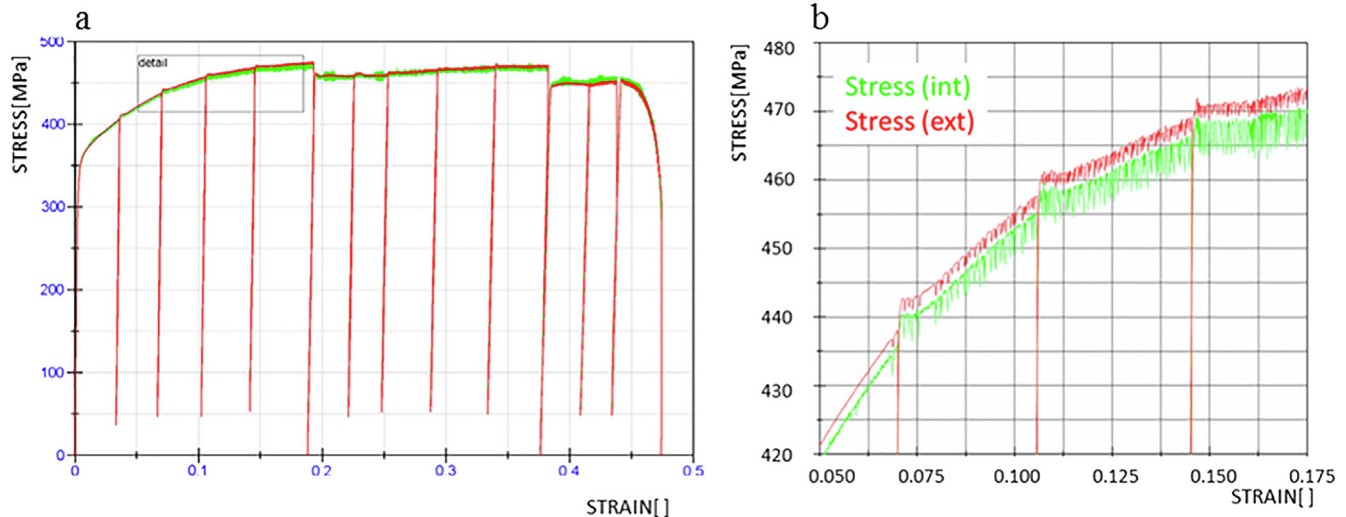


**Fig. 7.** a) Stress–strain curve for OFE Cu flat specimen at 4.2 K; b) in the zoom window red and green curves correspond to the load transducer outside and inside the cryostat. (For interpretation of the references to colour in this figure legend, the reader is referred to the web version of this article.)

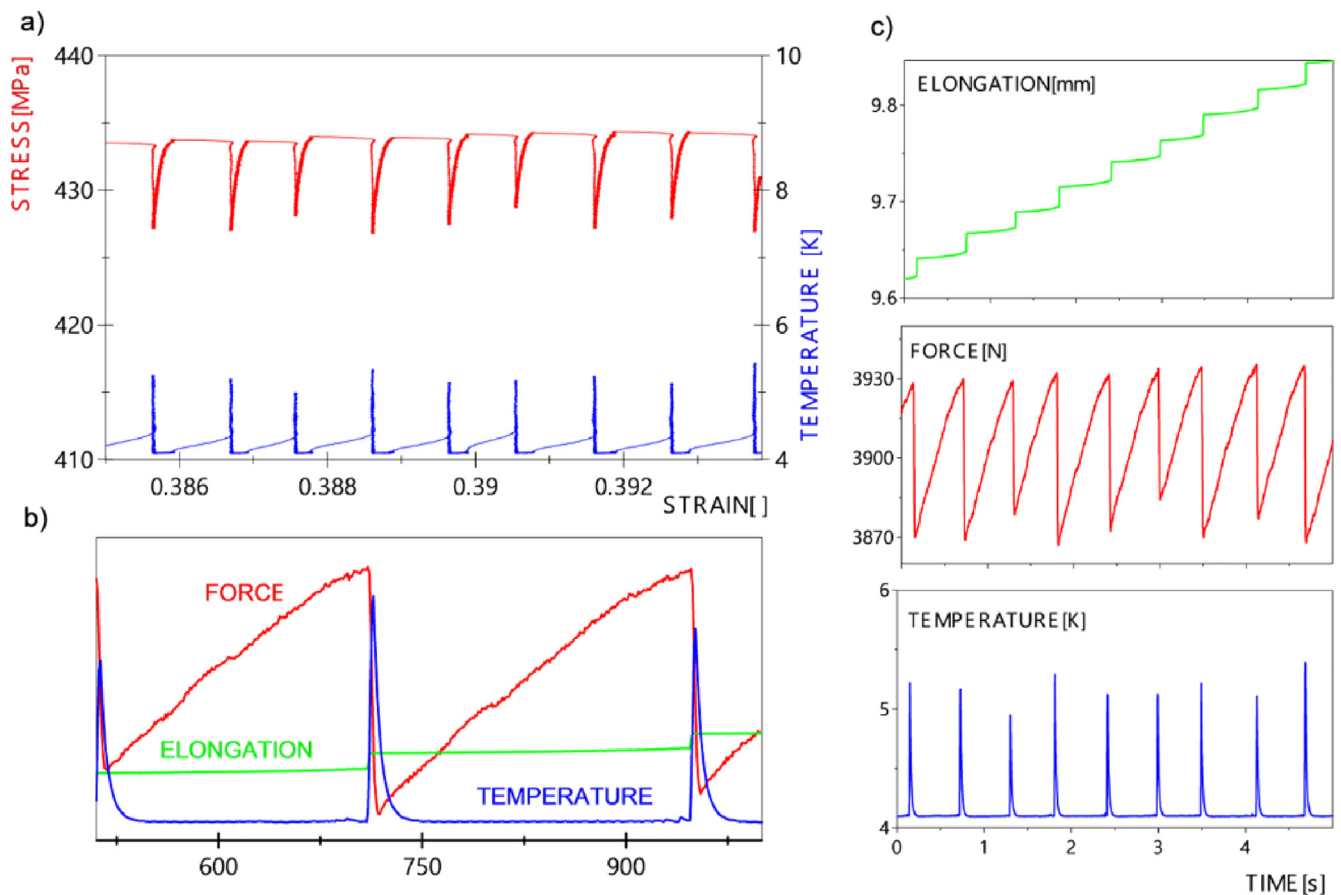


**Fig. 8.** Serrated yielding in OFE Cu flat specimen at 4.2 K: a) stress – strain and temperature – strain responses; b), c) decomposition of single serraion into force, elongation and temperature as a function of time.

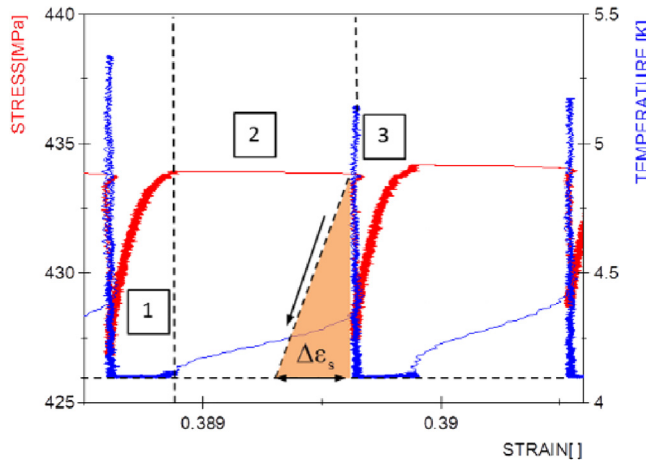


**Fig. 9.** Single serration during the uniaxial tensile test of OFE Cu at 4.2 K; the result of kinematically controlled tensile test; illustration of the amount of slip  $\Delta\epsilon_s$  during the process of catastrophic failure of lattice barriers.

The experimental results indicate that during the test, the typically full-size serrations in the NbTi filaments were combined with the gentle serrations in the copper matrix. Moreover, the DPF in the matrix was observed at the final stage of the uniaxial tensile test (Fig. 11). It is worth pointing out, that DPF is macroscopically reflected by the temperature distribution. In the composite specimen the peaks of temperature generated during DPF in the filaments are much higher than those generated by the matrix (blue curve in Fig. 12b).

## 5. Computational aspect of DPF in superconducting multifilament composites

Previously developed numerical model (Skoczeń et al., 2014; Tabin et al., 2016, 2017, 2019) is adopted to describe the DPF in the superconducting multifilament composite. The explicit incremental scheme (Forward Euler Method) was applied for the stress integration, controlled with a constant value of the total strain increment. The model assumes that DPF takes place independently in the NbTi filaments and in the OFE Cu matrix. The response of stress during the kinematically controlled uniaxial tensile test was defined for the composite specimen in terms of three stages

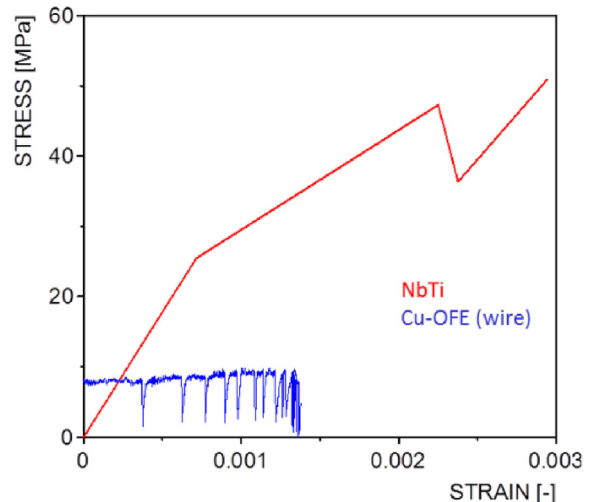


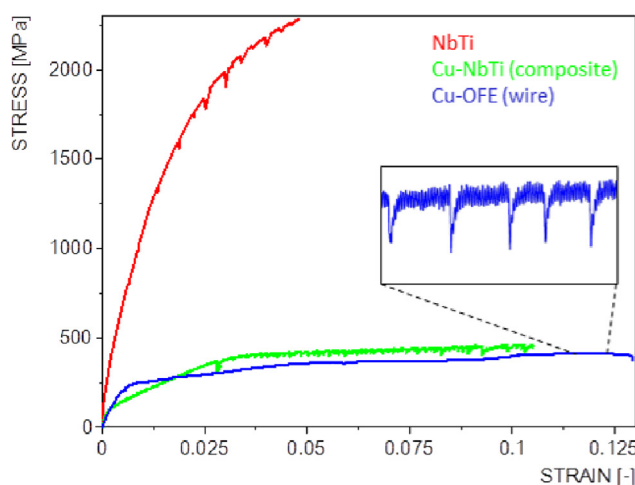
**Fig. 11.** Stress amplitude of single serrations in OFE Cu (blue) and NbTi (red) (Koch and Easton, 1977). (For interpretation of the references to colour in this figure legend, the reader is referred to the web version of this article.)

within each serration cycle: elastic loading (1), smooth plastic flow (2), abrupt drop of stress (3). Experimental results show that large serrations come from DPF process in the filaments, while the smaller ones come from the matrix. The earliest serrations are observed in the filaments, and then in the matrix, despite the fact that the copper matrix reached the yield stress before the NbTi filaments.

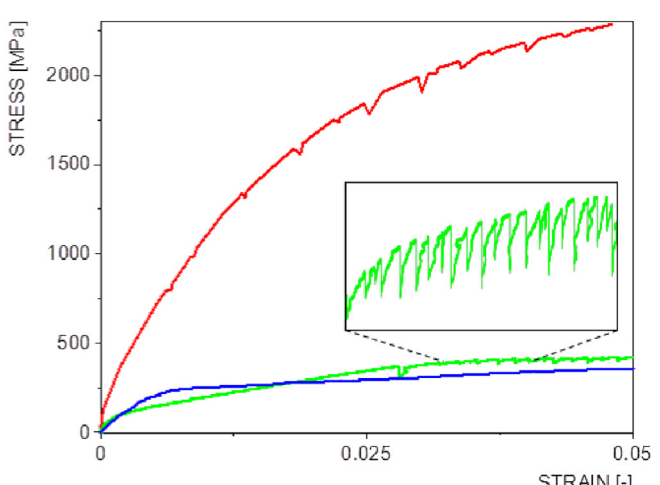
The model assumes that the increase of the plastic strain due to stage 3 (fast slip) is caused by a different mechanism (see Fig. 13c) than in the regular continuous yielding within stage 2 (motion of dislocations). Moreover, following the experimental results, it is assumed that the abrupt drop of stress (stage 3) occurs at a constant value of total strain. Hence, the redistribution of the elastic and the plastic parts of strain takes place in the stage 3 (Fig. 13).

In order to calculate the equivalent tangent modulus of multifilament composite during DPF, the two approaches were used, namely the homogenization method and the mixing law (Fig. 14).

The equivalent tangent moduli were obtained for each range of the deformation during the tensile test (Table 3). Elastic behaviour of the composite is described by the elastic-elastic effective modulus. Then, the plastic deformation starts in the matrix whereas the



**Fig. 10.** Stress-strain curves for NbTi wire, OFE Cu wire and Cu-NbTi composite obtained during kinematically controlled tests at 4.2 K.



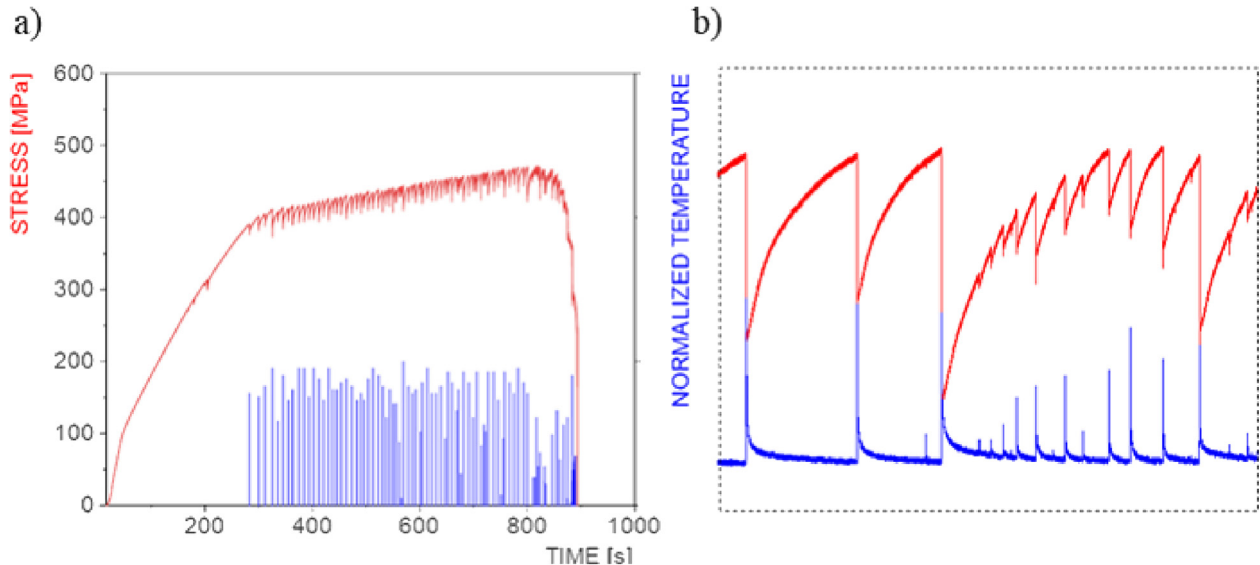


**Fig. 12.** DPF in the superconducting multifilament composite Cu-NbTi, during the kinematically controlled tensile test at 4.2 K.

**Table 2**  
Experimentally identified mechanical parameters of Cu-NbTi.

	$E_0$ [Pa]	$\sigma_{01}$ [Pa]	$\sigma_{02}$ [Pa]	$E_{h1}$ [Pa]	$E_{h2}$ [Pa]
<b>Cu NbTi</b>	$0.60 \cdot 10^{11}$	$1.00 \cdot 10^8$	$3.66 \cdot 10^8$	$0.135 \cdot 10^{11}$	$0.0079 \cdot 10^{11}$

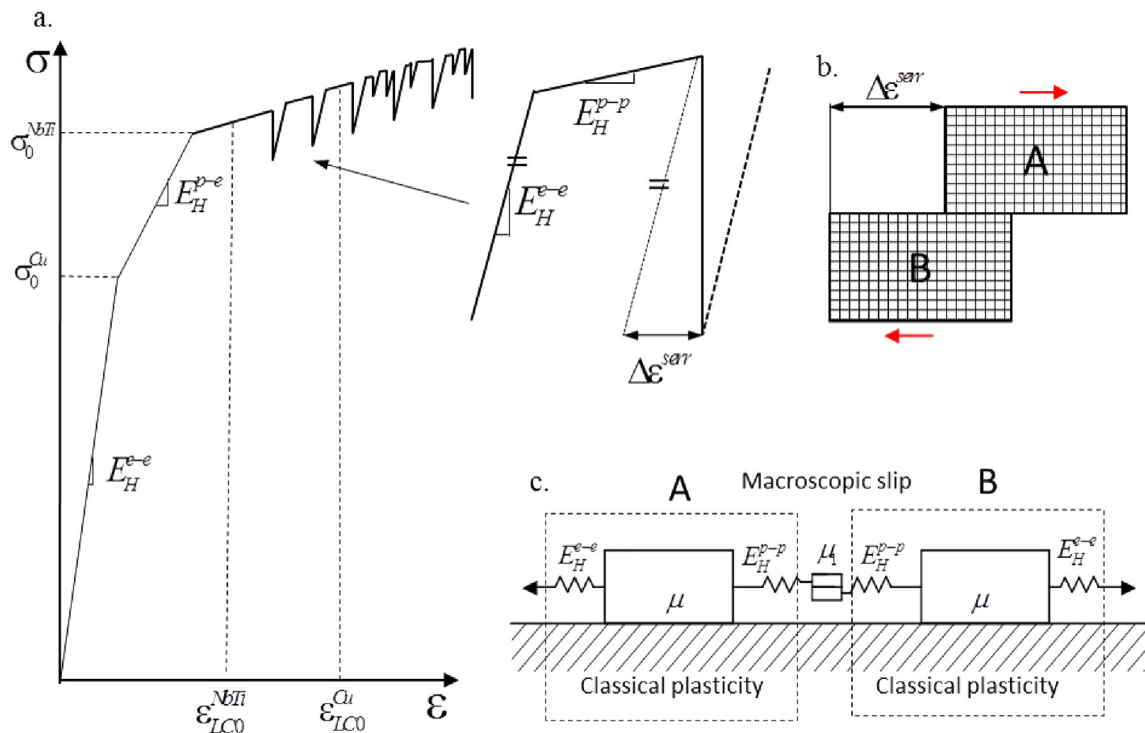


**Fig. 13.** a) Illustration of different mechanisms of the plastic deformation during DPF (Skoczeń, 2008, 2010); b) the amount of slip  $\Delta\epsilon^{serr}$  during the process of catastrophic failure of the lattice barriers; c) redistribution of plastic strain within one serration.

filaments remain still elastic. Thus the composite specimen is described by the plastic-elastic effective modulus. After the yield stress of the filaments is reached the composite is described by the plastic-plastic modulus.

General scheme of the numerical algorithm of DPF is presented in (Skoczeń et al., 2010; Skoczeń et al., 2014; Tabin et al., 2016, 2017, 2019), therefore identification of the effective tangent moduli is presented in this paper as well as the experimentally identi-

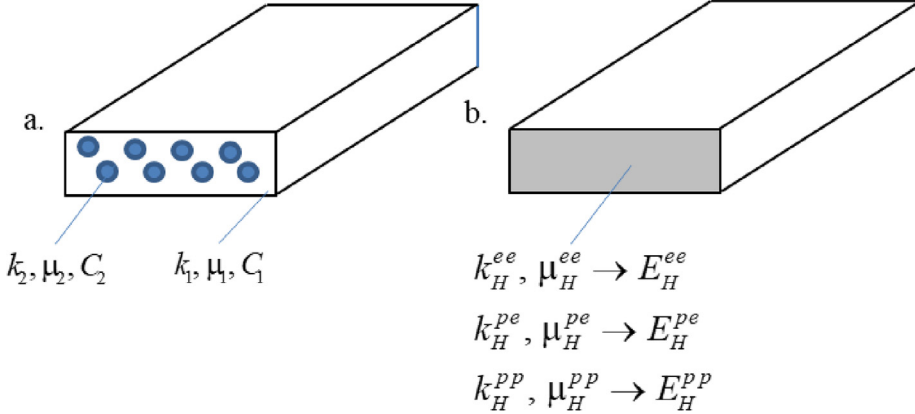


**Fig. 14.** a) Material parameters of the filaments and the matrix, b) the equivalent modulus of composite calculated by means of the Mori-Tanaka homogenization scheme.

**Table 3**

General equations of equivalent tangent moduli of multifilament composite.

Tangent equivalent modulus	Mori-Tanaka homogenization scheme	Extra parameters
elastic-elastic	$E_H^{ee} = k_H^{ee} + 2\mu_H^{ee}$	
plastic-elastic	$E_H^{pe} = k_H^{pe} + 2\mu_H^{pe}$	$\eta_1 = \frac{C_1}{E_1 + C_1}$
plastic-plastic	$E_H^{pp} = k_H^{pp} + 2\mu_H^{pp}$	$\eta_2 = \frac{C_2}{E_2 + C_2}$

**Table 4**

Parameters of numerical model of DPF in the multifilament composite.

parameter	Units	Cu OFE	NbTi filament
$E_0$	elastic modulus	Pa	$0.45 \cdot 10^{11}$
$E_h$	hardening modulus	Pa	$14.50 \cdot 10^8$
$\nu$	Poisson's ratio	—	0.35
$\sigma_0$	initial yield stress value	Pa	$2.50 \cdot 10^8$
$\rho_0$	density of dislocations	$1/m^2$	$3.0 \cdot 10^{12}$
$B_0$	initial value of density of the lattice barriers	$1/m^2$	$5.0 \cdot 10^{11}$
$\tau_0$	internal lattice friction	Pa	$\frac{\sigma_0}{M}$
$\mu$	shear modulus	Pa	$\frac{E_0}{2(1+\nu)}$
$k$	bulk modulus	Pa	$\frac{E_0}{3(1-2\nu)}$
$b$	length of the Burgers vector	m	$2.58 \cdot 10^{-10}$
$d$	average grain size	m	$2.5 \cdot 10^{-6}$
$M$	Taylor's constant	—	3.0
$\alpha$	dislocations interaction factor	—	0.4
$k_{c1}$	constant	—	0.031
$k_{c2}$	constant	—	0.002
$k_a$	dislocation annihilation constant	—	0.01
$p_{B0}$	initial plastic strain threshold for the evolution of the lattice barriers	—	0.0651
	plastic strain when first serrations are observed	—	0.075 (flat specimen) 0.083 (composite)
$\Delta p_B$	variable increment of the threshold for the evolution of the lattice barriers;	—	0.0005 0.018 (cylindrical specimen) 0.028 (composite) −0.05 $p_B$

fied mechanical properties and material parameters of the Cu matrix and the NbTi filaments are shown. The numerical results were obtained for the following set of parameters:

Some of the parameters in Table 4 come from the literature position (Koch and Easton, 1977; Schmidt, 1978). Some of them were identified during tensile test at 4.2 K (Skoczeń, 2004;

Skoczeń et al., 2010) and a few were chosen to calibrate the numerical model.

Based on the Mori-Tanaka homogenization scheme and the material parameters the following equivalent effective moduli were obtained for the Cu-NbTi specimen:

Having determined the effective tangent moduli (Table 5), the linear stress increment is calculated for each strain increment  $\Delta\epsilon$ ,

**Table 5**  
Equivalent effective moduli for Cu-NbTi.

elastic-elastic [Pa]	plastic-elastic [Pa]	plastic-plastic [Pa]
$k_H^{ee} = 0.534 \cdot 10^{11}$	$k_H^{pe} = 0.0194 \cdot 10^{11}$	$k_H^{pp} = 0.0190 \cdot 10^{11}$
$\mu_H^{ee} = 0.200 \cdot 10^{11}$	$\mu_H^{pe} = 0.0071 \cdot 10^{11}$	$\mu_H^{pp} = 0.0069 \cdot 10^{11}$
$E_H^{ee} = 0.934 \cdot 10^{11}$	$E_H^{pe} = 0.0335 \cdot 10^{11}$	$E_H^{pp} = 0.0328 \cdot 10^{11}$

with the effective tangent modulus depending on the deformation stage in the filaments and the matrix (36):

$$\Delta\sigma_{\text{comp}} = E_H^{ij}\Delta\epsilon, \quad i,j = e, p \quad (55)$$

Alternatively, the mixing law, based on the section equilibrium condition, may be used to obtain the stress-strain relation for the composite. After the integration algorithm is applied separately for Cu (matrix) and NbTi (filaments), the effective stress in composite is calculated for each total strain value (the same for Cu and NbTi):

$$\sigma_{\text{comp}} = \xi_{\text{Cu}}\sigma_{\text{Cu}} + \xi_{\text{NbTi}}\sigma_{\text{NbTi}} \quad \xi_{\text{Cu}} + \xi_{\text{NbTi}} = 1 \quad (54)$$

The mixing law is applied for the estimation of serrations in the both above approaches.

The results of numerical simulation of DPF for the OFE Cu flat specimen, the NbTi wire and the superconducting multifilament

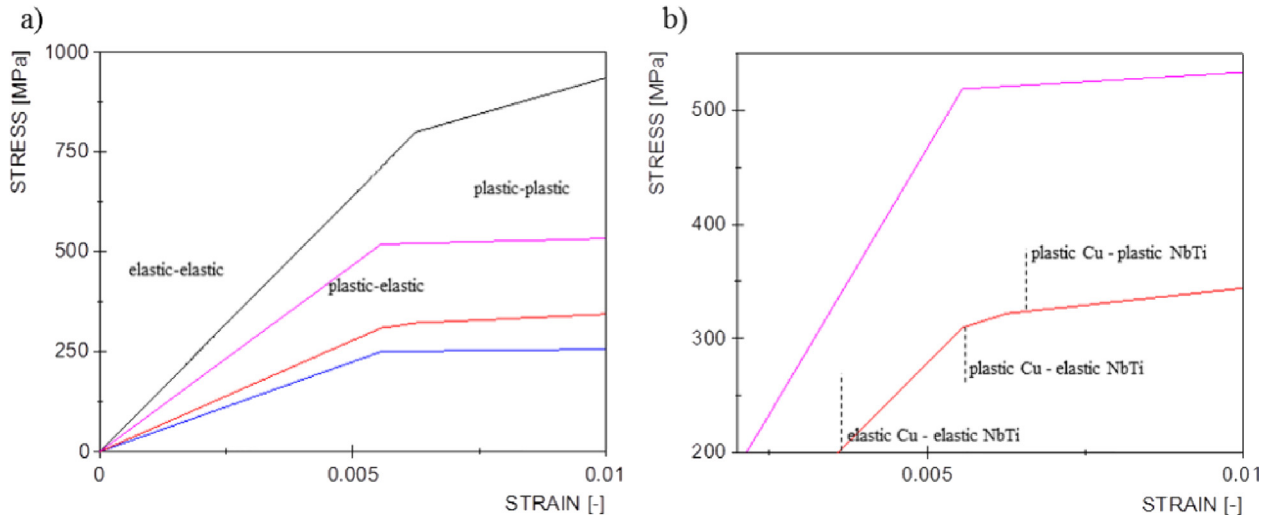


Fig. 15. Tri-linear initial equilibrium curves for composite: elastic-elastic, plastic-elastic, plastic-plastic.

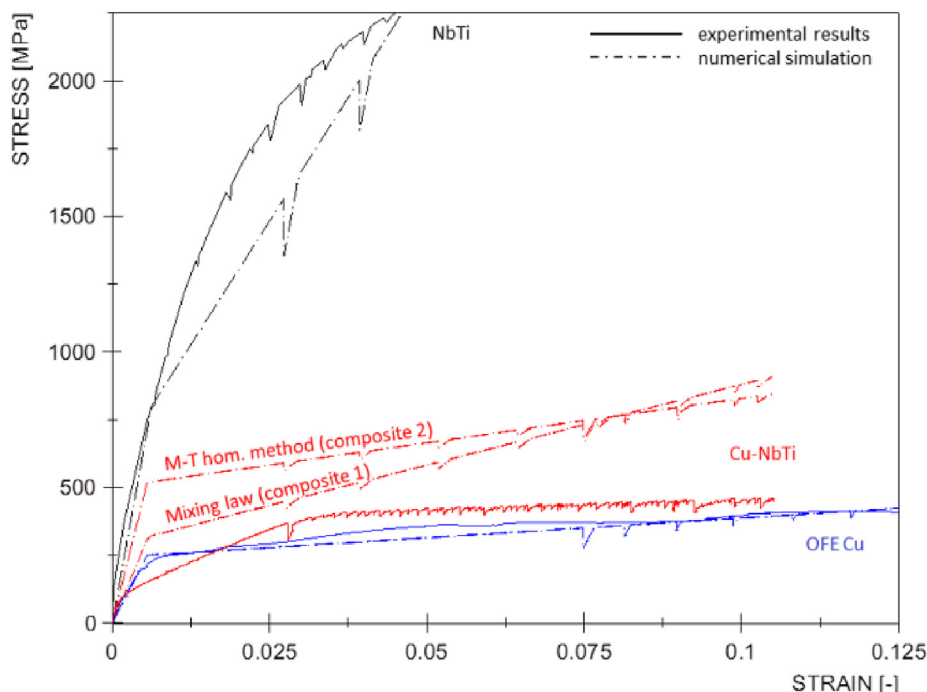


Fig. 16. Experimental results versus numerical simulation: stress-strain curves for NbTi, OFE Cu and Cu-NbTi.

composite are presented in Figs. 15 and 16. The result of the mixing law applied is denoted Composite (1), and of the effective tangent moduli – Composite (2). The computed stress-strain curves for OFE Cu and NbTi exhibit good correlation with the experimental data obtained during the kinematically controlled uniaxial tensile test at 4.2 K.

## 6. Discussion

The superconducting multifilament composite composed of the copper matrix and the unidirectional long fibres (strands) has been tested at extremely low temperatures (liquid helium, 4.2 K) in order to verify the type of inelastic behaviour, both in the matrix and in the fibres. It turns out that the so-called discontinuous plastic flow (DPF) is observed both in the copper matrix and in the superconducting fibres (strands), however, their behaviour in terms of hardening, the frequency and the amplitude of drop of stress is quite different, which is certainly motivated by different chemical composition and microstructure of both components. In particular, the copper matrix exhibits quite frequent oscillations of stress against strain (or time), however their amplitude is not very large (of the order of 5 MPa). The stress oscillations are accompanied by the oscillations of temperature, which is justified by the so-called thermodynamic instability (see Chapter 2). It has been clearly shown, that the specific heat tends to zero with temperature, which leads to the conclusion that the derivative of temperature with respect to heat ( $dT/dQ$ ) tends to infinity with temperature approaching absolute zero (Eq. 4). This becomes the main cause of the thermodynamic instability, associated directly with the phenomenon of adiabatic heating. The process of plastic slip in the matrix generates local dissipation of energy in the primary form of plastic power. As a result of conversion of plastic power to heat in the nearly adiabatic conditions (the thermal conductivity tends to zero with temperature), the temperature rise is observed. The temperature spikes may reach some 2–4 K in the case of copper, and they are systematically correlated to the drops of stress. The behaviour of copper matrix at very low temperatures (liquid helium) is therefore discontinuous by nature, as long as the process is kinematically controlled. Similar behaviour is observed in the case of NbTi fibres (strands), that show the same type of mechanical response, even if the frequency of stress against strain oscillations is much smaller and the amplitude of drops of stress is much larger (of the order of 20 MPa or more) than in the case of copper. Also, the NbTi fibres exhibit much higher hardening when compared to copper, which has strong influence on the behaviour of the entire composite (Fig. 12). As a result of discontinuous plastic flow in the matrix and in the fibres, the resulting behaviour of the composite in terms of plastic flow is also discontinuous. Moreover, the composite is characterized by frequent and small (in terms of amplitude) stress oscillations due to the behaviour of copper, and less frequent but large stress oscillations due to the behaviour of fibres (strands). This makes the response of the whole composite less regular and more complex for the constitutive and the numerical modelling. In the present paper, an improved constitutive model of the discontinuous plastic flow, when compared to the model developed in the previous papers, has been applied. Moreover, the model has been applied in the entirely new circumstances given the fact that the matrix and the fibres are connected to each other by an interface that is not coherent, however, it is able to carry the longitudinal tangent loads. In the primary approach, the Bernoulli hypothesis of flat cross-sections has been applied, which leads to the same strain in the matrix and in the fibres within the same cross-section. Initially, the mixing law has been applied in order to apportion the stress components to the matrix and to the fibres. The mixing law, even if

very simple, allows to represent the serrations both in the matrix and in the fibres, and to obtain rather complete representation of the behaviour of the whole composite. Thus, frequent serrations of small amplitude in the copper matrix are accompanied by rare serrations of large amplitude in the fibres, which fits well to the behaviour of the composite during the low temperature tests. Such a model is regarded as the first, and rather basic approach.

In order to proceed further and to develop more precise model, the mean field methods were applied. In particular, the Mori-Tanaka homogenization scheme has been adopted in order to compute the overall tangent stiffness of the composite containing the superconducting fibres. The Mori-Tanaka homogenization scheme is explicit, therefore the overall tangent stiffness is computed in one go. Moreover, it is suitable in all the cases where the volume fraction of secondary component is much smaller when compared to the volume fraction of primary component (the matrix), which is the case of the unidirectional copper stabilized superconductors. In order to represent all possible cases, the following states were taken into account (matrix/fibres): elastic-elastic (1), plastic-elastic (2), elastic-plastic (3), plastic-plastic (4). It is worth pointing out that two first cases (1,2) were already derived in the previous papers (Ortwein et al., 2014; Ryś and Skoczeń, 2017; Skoczeń, 2007) with respect to the phase transformation process, where the primary phase was elastic or plastic, and the secondary phase was elastic. In the present paper, an entirely new plastic-plastic case has been added, that represents simultaneous plastic behaviour in both components of the composite. This means that in both cases (matrix and fibres) the tangent stiffness operator has been derived in its full anisotropic form, containing dyadic product of the vectors normal to the yield surfaces. In order to obtain simpler form of the tangent stiffness operator, its projection to the space of isotropic operators has been performed. As a result, the dyadic product of the vectors normal to the yield surfaces has been reduced, whereas the shear and the bulk moduli were simultaneously enriched by the tangent stiffness modulus computed by means of the elastic and the hardening moduli, for each component (matrix/fibre) separately. This linearization allows to apply the Mori-Tanaka homogenization scheme at each stage of the deformation process, since both components have their own isotropic representation of the tangent stiffness operator. Thus, all the above mentioned cases (1–4) can be efficiently solved. In the case of soft copper matrix and much stiffer superconducting fibres, the following states are active (matrix/fibre): elastic-elastic, plastic-elastic and plastic-plastic. Given the fact, that the proportion between the matrix and the fibres does not change during the deformation process, the above approach leads to a piecewise linear representation of the composite, containing both small and large serrations. Such a representation fits reasonably well to the experimental results (Fig. 16), where the piecewise linear behaviour of the composite is well visible. It is worth pointing out that experimentally tested Cu-NbTi is subdivided into fine filaments, which are twisted together and embedded in a OFE Cu matrix. It is required to eliminate instabilities in the superconductor known as flux jumps. On the other hand, the filament twisting reduces the inter-filament coupling under time-varying fields, while cooper matrix (high thermal and current conductivity) is used as a current shunt in the case of transition of the filaments to the normal resistive state (so-called quench effect). Therefore, precise calibration of the numerical results versus the experimental data in terms of frequency and amplitude of serrations is rather difficult, that is why the results presented in the present paper have to be treated in a qualitative manner. Nevertheless, the very fact that both types of serrations were accommodated in the model, and the overall stiffness of the composite has been obtained by means of the mean field methods, makes this model quite promising in terms of physical representation of the phenomena that take place in the copper

matrix and in the superconducting fibres. Another problem that arises is linked to the fact, that the interface between the matrix and the fibres is not coherent, which might contribute to possible stick-slip effect in the interface. The stick-slip effect has, however, quite different appearance at the macroscopic level, and can be easily distinguished when compared to the classical serrations. More sophisticated method, that might help to distinguish between the stick-slip in the interface and the serrations (discontinuous plastic flow) is the acoustic emission that is currently being developed for extremely low temperatures. Finally, it is worth pointing out that the temperatures spikes measured in the course of the deformation process are precisely correlated with the drops of stress, as indicated in Fig. 12, which is an obvious result of the thermodynamic instability described in Chapter 2. In the present model, the thermodynamic coupling between the serrations (drops of stress) and resulting energy dissipation in the form of plastic power, accompanied by the temperature oscillations, was not taken into account and remains the matter of the future investigations.

Moreover the mechanism of discontinuous plastic flow (DPF, serrated yielding), that occurs at extremely low temperatures in fcc materials was explained in the context of uniaxial tensile test, what will happen during kinematically controlled combined loads and non-proportional loading paths? To this end, dedicated set-up is being developed. Based on this, the modelling of the fracture mechanisms in heterogeneous materials (multiphase and composite), subjected to multiaxial loads (proportional and nonproportional paths) at extremely low temperatures (liquid nitrogen 77 K, liquid helium 4.2 K, superfluid helium 1.9 K) will be considered.

## 7. Conclusions

The constitutive model discussed in the paper describes one of the fundamental dissipative phenomena that occur at very low temperatures – discontinuous plastic flow (DPF) in complex composite material. In order to describe the mechanical behaviour of a composite composed of matrix (OFE Cu) and the superconductor strands (NbTi, Nb<sub>3</sub>Sn) two approaches have been used: the mixing law and the mean field methods. The first one allows to represent the serrations both in the matrix and in the fibres, and to obtain complete representation of the behaviour of the whole composite. On the other hand, the Mori-Tanaka homogenization scheme (the mean field methods) has been adopted in order to compute the overall tangent stiffness of the composite containing the superconducting fibres.

Validation and verification of DPF model developed in the paper, have been carried out based on the uniaxial tensile tests of Cu-NbTi composite specimens. The experimental results indicate that the full-size serrations in the NbTi filaments were combined with the “gentle” serrations in the copper matrix. Moreover, the DPF in the matrix was observed at the final stage of the uniaxial tensile test (cf. Koch and Easton, 1977). It is worth pointing out, that DPF is reflected by the temperature distribution. In the composite specimen the temperature peaks generated during DPF in the filaments are much higher than generated in the matrix.

The constitutive model is physically based, and reflects all the important features of the DPF in the composite materials. Moreover, the model allows to reproduce the observed serrations both in the matrix and in the strands.

The superconducting multifilament composites (Cu-NbTi) are commonly used for the coils of the superconducting magnets in large scientific instruments, such as: Large Hadron Collider (LHC, Switzerland), Tevatron (USA) or magnetic resonance imaging

(MRI). Therefore, the following question has been raised: how to design the modern conductors in order to reduce the dissipative effects like DPF or the stick slip effect?

The heat released in the course of DPF process, due to thermodynamic instability, generates drastic increase of temperature, which can lead to resistive transition (quench) in the superconducting magnets. In order to describe correctly the mechanical behaviour of composite superconductors at extremely low temperatures, the constitutive model of DPF developed in the present paper can be successfully used.

## Acknowledgements

This work has been supported by the National Science Centre through the Grant No. UMO-2016/21/N/ST8/02368.

## References

- Basinski, Z.S., 1957. The instability of plastic flow of metals at very low temperatures. *Proc. R. Soc. Lond. Ser. A* 240, 229–242.
- Bauer, P., Rajainmaki, H., Salpietro, E., 2007. EFDA Material Data Compilation for Superconductor Simulation. EFDA CSU, Garching.
- Devred, A., 2004. Practical Low-Temperature Superconductors for Electromagnets, in: Monographs), C.Y.R. (Ed.), CERN, Geneva, CERN.
- Gu, T., Medy, J.R., Volpi, F., Castelnau, O., Forest, S., Hervé-Luanco, E., Lecouturier, F., Proudhon, H., Renault, P.O., Thilly, L., 2017. Multiscale modeling of the anisotropic electrical conductivity of architected and nanostructured Cu-Nb composite wires and experimental comparison. *Acta Mater.* 141, 131–141.
- Gu, T., Medy, J.R., Klosek, V., Castelnau, O., Forest, S., Hervé-Luanco, E., Lecouturier-Dupouy, F., Proudhon, H., Renault, P.O., Thilly, L., Villechaise, P., 2019. Multiscale modeling of the elasto-plastic behavior of architected and nanostructured Cu-Nb composite wires and comparison with neutron diffraction experiments. *Int. J. Plast.* 122, 1–30.
- Koch, C.C., Easton, D.S., 1977. A review of mechanical behaviour and stress effects in hard superconductors. *Cryogenics* 17, 391–413.
- Kocks, U.F., Mecking, H., 2003. Physics and phenomenology of strain hardening: the FCC case. *Prog. Mater. Sci.* 48, 171–273.
- Marquardt, E.D., Le, J.P., Radebaugh, R., 2000. Cryogenic material properties database, in: the 11th International Cryocooler Conference, Keystone, Co.
- Mecking, H., Kocks, U.F., 1981. Kinetics of flow and strain-hardening. *Acta Metall.* 29, 1865–1875.
- Obst, B., Nyilas, A., 1991. Experimental evidence on the dislocation mechanism of serrated yielding in f.c.c. metals and alloys at low temperatures. *Mater. Sci. Eng., A* 137, 141–150.
- Obst, B., Nyilas, A., 1998. Time-resolved flow stress behavior of structural materials at low temperatures. *Advances in Cryogenic Engineering* 44, 331–338.
- Ortwein, R., Skoczeń, B., Tock, J.P., 2014. Micromechanics based constitutive modeling of martensitic transformation in metastable materials subjected to torsion at cryogenic temperatures. *Int. J. Plast.* 59, 152–179.
- Pustovalov, V.V., 2008. Serrated deformation of metals and alloys at low temperatures (Review). *Low Temp. Phys.* 34, 683–723.
- Read, D.T., 1978. Metallurgical effects in niobium-titanium alloys. *Cryogenics* 18, 579–584.
- Reed, R.P., McCowan, C.N., Walsh, R.P., Delgado, L.A., McCloskey, J.D., 1988. Tensile strength and ductility of indium. *Mater. Sci. Eng., A* 102, 227–236.
- Reed, R.P., Walsh, R.P., 1988. Tensile strain rate effect in liquid helium. *Adv. Cryogenic Eng. Mater.* 34, 199–208.
- Rossi, L., Sorbi, M., 2006. MATPRO: A Computer Library of Material Property at Cryogenic Temperature. CARE-Note-2005-018-HHH, Superconductors Database.
- Ryś, M., Skoczeń, B., 2017. Coupled constitutive model of damage affected two-phase continuum. *Mech. Mater.* 115, 1–15.
- Schmidt, C., 1978. The induction of a propagating normal zone (quench) in a superconductor by local energy release. *Cryogenics* 18, 605–610.
- Schwarz, R.B., Mitchell, J.W., 1974. Dynamic dislocation phenomena in single crystals of Cu-10.5-at.-%-Al alloys at 4.2 K. *Phys. Rev. B* 9, 3292–3299.
- Seeger, A., 1957. Dislocations and mechanical properties of crystals. Wiley, New York.
- Shin, J.K., Ochiai, S., Sugano, M., Okuda, H., Nyilas, A., Oh, S.S., 2008. Direct measurement of difference in local deformation and its influence on critical current in Bi2223/Ag/Ag alloy composite tape. *Scr. Mater.* 59, 448–450.
- Skoczeń, B., 2004. Compensation Systems for Low Temperature Application. Springer-Verlag, Berlin.
- Skoczeń, B., 2007. Functionally graded structural members obtained via the low temperature strain induced phase transformation. *Int. J. Solids Struct.* 44, 5182–5207.
- Skoczeń, B., 2008. Constitutive model of plastic strain induced phenomena at cryogenic temperatures. *J. Theoret. Appl. Mech.* 46, 949–971.
- Skoczeń, B., Bielski, J., Sgobba, S., Marcinek, D., 2010. Constitutive model of discontinuous plastic flow at cryogenic temperatures. *Int. J. Plast.* 26, 1659–1679.

- Skoczeń, B., Bielski, J., Tabin, J., 2014. Multiaxial constitutive model of discontinuous plastic flow at cryogenic temperatures. *Int. J. Plast.* 55, 198–218.
- Tabachnikova, E.D., Dolgin, A.M., Bengus, V.Z., Yefimov, Y.V., 1984. *Fiz. Metallovedenie* 58.
- Tabin, J., Prąćik, M., 2015. Methods for identifying dynamic parameters of clip-on extensometer-specimen structure in tensile tests. *Measurement* 63, 176–186.
- Tabin, J., Skoczen, B., Bielski, J., 2016. Strain localization during discontinuous plastic flow at extremely low temperatures. *Int. J. Solids Struct.* 97–98, 593–612.
- Tabin, J., Skoczen, B., Bielski, J., 2017. Damage affected discontinuous plastic flow (DPF). *Mech. Mater.* 110, 44–58.
- Tabin, J., Skoczen, B., Bielski, J., 2019. Discontinuous plastic flow coupled with strain induced fcc–bcc phase transformation at extremely low temperatures. *Mech. Mater.* 129, 23–40.
- Thilly, L., Petegem, S.V., Renault, P.-O., Lecouturier, F., Vidal, V., Schmitt, B., Swygenhoven, H.V., 2009. A new criterion for elasto-plastic transition in nanomaterials: application to size and composite effects on Cu–Nb nanocomposite wires. *Acta Mater.* 57, 3157–3169.
- Tock, J.P., Bozzini, D., Laurent, F., Russenschuck, S., Skoczeń, B., 2004. Electromechanical aspects of the interconnection of the LHC superconducting corrector magnets. *LHC Project Report* 724.
- Vidal, V., Thilly, L., Van Petegem, S., Stuhr, U., Lecouturier, F., Renault, P.O., Van Swygenhoven, H., 2009. Plasticity of nanostructured Cu–Nb-based wires: strengthening mechanisms revealed by *in situ* deformation under neutrons. *Scr. Mater.* 60, 171–174.
- Wessel, E.T., 1957. Metals at low temperatures. *Trans. ASM* 49, 149.
- Zaiser, M., Hahner, P., 1997. Oscillatory Modes of Plastic Deformation: Theoretical Concepts. *physica status solidi (b)* 199, 267–330.
- Zhang, P., Li, J., Guo, Q., Zhu, Y., Yan, K., Wang, R., Zhang, K., Liu, X., Feng, Y., 2019. Chapter 15 – NbTi superconducting wires and applications. In: Froes, F., Qian, M., Niinomi, M. (Eds.), *Titanium for Consumer Applications*. Elsevier, pp. 279–296.